The Astrophysical Journal, 665: L1–L4, 2007 August 10

BAYESIAN ANALYSIS OF THE LOW-RESOLUTION POLARIZED 3 YEAR *WMAP* SKY MAPS

H. K. Eriksen,[1,2] Greg Huey,[3,4,5] A. J. Banday,[6] K. M. Górski,[4,5,7] J. B. Jewell,[3,4]
I. J. O'Dwyer,[3,4] and B. D. Wandelt[3,6,8]

Received 2007 May 24; accepted 2007 June 27; published 2007 July 31

ABSTRACT

We apply a previously developed Gibbs sampling framework to the foreground-corrected 3 yr *WMAP* polarization data and compute the power spectrum and residual foreground template amplitude posterior distributions. We first analyze the co-added Q- and V-band data, and compare our results to the likelihood code published by the *WMAP* team. We find good agreement, and thus verify the numerics and data-processing steps of both approaches. However, we also analyze the Q- and V-band data separately, allowing for nonzero *EB* cross-correlations and including two individual foreground template amplitudes tracing synchrotron and dust emission. In these analyses, we find tentative evidence of systematics: The foreground tracers correlate with each of the Q- and V-band sky maps individually, although not with the co-added QV map; there is a noticeable negative *EB* cross-correlation at $l \lesssim 16$ in the V-band map; and finally, when relaxing the constraints on *EB* and *BB*, noticeable differences are observed between the marginalized band powers in the Q and V bands. Further studies of these features are imperative, given the importance of the low-*l EE* spectrum on the optical depth of reionization τ and the spectral index of scalar perturbations n_s.

Subject headings: cosmic microwave background — cosmology: observations — methods: numerical

1. INTRODUCTION

One of the most remarkable results in the 3 yr data release from the *Wilkinson Microwave Anisotropy Probe* (*WMAP*) experiment (Hinshaw et al. 2007; Page et al. 2007) was the detection of large-scale *E*-mode polarization at millimeter wavelengths. This was interpreted as the theoretically predicted signature of reionization, and allowed the *WMAP* team to set new and tighter constraints on the optical depth of reionization τ. In turn, the well-known degeneracy between τ and the spectral index of primordial scalar perturbations n_s was broken. The final outcome was a claimed detection of $n_s \neq 1$ at a statistical significance of almost 3 σ (Spergel et al. 2007).

One should bear in mind, however, the great potential for systematic effects in both the temperature and polarization measurements. For instance, the precise level of power contribution from unresolved point sources affects n_s directly. An independent analysis of this particular issue by Huffenberger et al. (2006) showed that the initial point-source amplitude quoted by the *WMAP* team was indeed too high, which biased n_s to low values. Similarly, on large scales the likelihood approximation used by the *WMAP* team was biased high (Eriksen et al. 2006), which also biased n_s low. After these corrections, the statistical significance of $n_s \neq 1$ dropped to ~ 2 σ.

For polarization the situation may be even more serious due to the strong sensitivity of τ and n_s on the low-*l EE* spectrum, combined with the low signal-to-noise ratio of the *WMAP* data. Systematic effects, both from the instrument itself (Jarosik et al. 2007) and from noncosmological foregrounds (Kogut et al. 2007), are much more likely to affect the results, and we are also much less likely to detect them. It is therefore imperative to carefully check both the data and the analysis methods, in order to build up confidence in the final cosmological results. In this Letter, we start this task by computing the low-*l EE*, *EB*, *BB*, and foreground template amplitude posterior distributions from the *WMAP* data.

2. METHOD

We use a previously introduced Gibbs sampling framework (Jewell et al. 2004; Wandelt et al. 2004; Eriksen et al. 2004; Larson et al. 2007) to estimate the posterior distributions. For full details on the method, we refer the interested reader to the quoted papers, and only summarize the principles here.

First we define our notation. The desired distribution is denoted $P(\boldsymbol{s}, C_l, \boldsymbol{f}\,|\,\boldsymbol{d})$, where $\boldsymbol{s}$ is the CMB signal, $C_l = \{C_l^{EE}, C_l^{EB}, C_l^{BB}\}$ is the CMB power spectrum, $\boldsymbol{f}$ is a set of foreground template amplitudes, and $\boldsymbol{d}$ are the data.

The Gibbs sampler is a Markov Chain Monte Carlo method and, as such, maps out the full posterior by drawing samples from it. While direct evaluation or sampling from the posterior $P(C_l|\boldsymbol{d})$ requires inversion of a prohibitively large matrix, the Gibbs sampling scheme (Gelfand & Smith 1990) uses the conditional densities of the joint posterior $P(C_l, \boldsymbol{s}|\boldsymbol{d})$, which is computationally feasible to sample from. The algorithm may thus be described by the following sampling steps:

$$\boldsymbol{s}^{i+1} \leftarrow P(\boldsymbol{s}|C_l^i, \boldsymbol{f}^i, \boldsymbol{d}), \tag{1}$$

$$C_l^{i+1} \leftarrow P(C_l|\boldsymbol{s}^{i+1}, \boldsymbol{f}^i, \boldsymbol{d}), \tag{2}$$

$$\boldsymbol{f}^{i+1} \leftarrow P(\boldsymbol{f}|\boldsymbol{s}^{i+1}, C_l^{i+1}, \boldsymbol{d}). \tag{3}$$

Here the symbol $\leftarrow$ indicates sampling from the conditional distribution on the right-hand side, which can be accomplished without inverting the signal-plus-noise covariance matrix (for details, see Jewell et al. 2004; Wandelt et al. 2004; Eriksen et al. 2004; Larson et al. 2007). For the foreground template amplitude distribution, we note that the required algorithm is

[1] Institute of Theoretical Astrophysics, University of Oslo, P.O. Box 1029 Blindern, N-0315 Oslo, Norway; h.k.k.eriksen@astro.uio.no.
[2] Centre of Mathematics for Applications, University of Oslo, P.O. Box 1053 Blindern, N-0316 Oslo, Norway.
[3] Department of Physics, University of Illinois, Urbana, IL 61801.
[4] Jet Propulsion Laboratory, 4800 Oak Grove Drive, Pasadena, CA 91109.
[5] California Institute of Technology, Pasadena, CA 91125.
[6] Max-Planck-Institut für Astrophysik, Karl-Schwarzschild-Strasse 1, Postfach 1317, D-85741 Garching bei München, Germany.
[7] Warsaw University Observatory, Aleje Ujazdowskie 4, 00-478 Warsaw, Poland.
[8] Astronomy Department, University of Illinois, Urbana, IL 61801-3080.

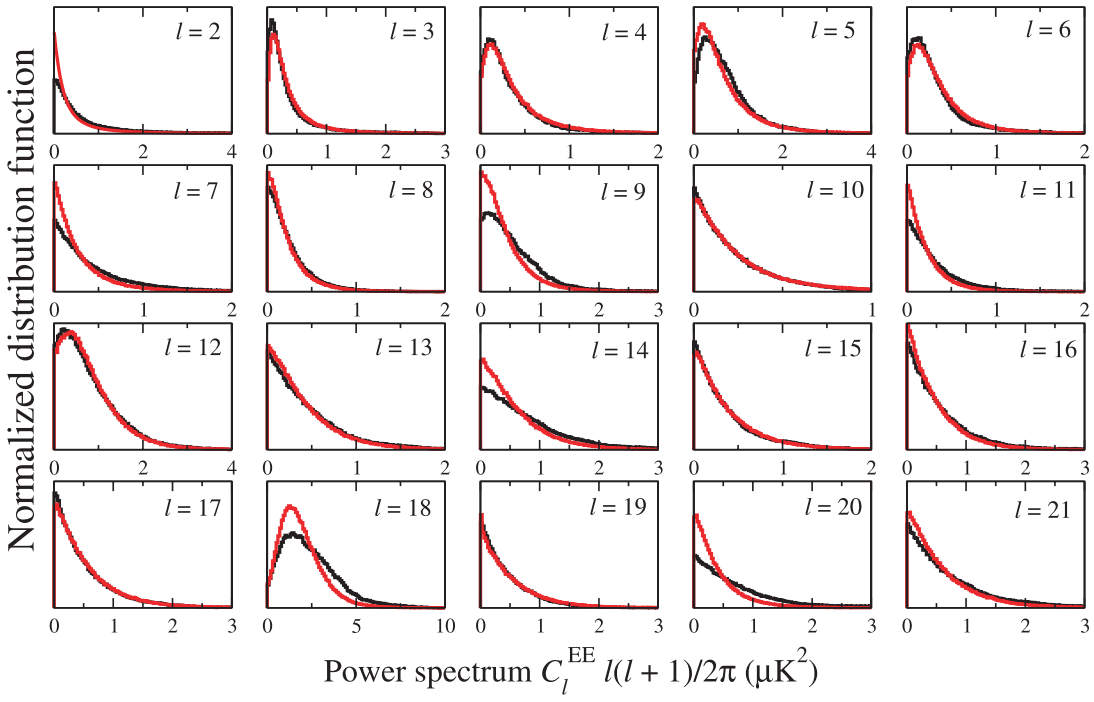

FIG. 1.—Comparison of single-*l* *EE* marginal posteriors from the *WMAP* code (*black distributions*) and the Gibbs sampler (*red distributions*) using the QV map. The *EB* and *BB* power spectra are held at zero.

identical to that employed for sampling monopole and dipole amplitudes (Eriksen et al. 2004).

3. DATA

We consider only the low-resolution foreground-corrected 3 yr *WMAP* polarization data in this Letter, as provided on LAMBDA.[9] These come in the form of three HEALPix[10] sky maps, pixelized at $N_{\rm side} = 16$, each having 3072 pixels in both Stoke's *Q* and *U*. The *WMAP* P06 sky cut is imposed on the data, leaving only 2267 pixels for the analysis. Two frequency bands are included, namely the Q band (41 GHz) and V band (61 GHz). In addition, we analyze the co-added map (denoted QV), and also the two frequency maps jointly but not co-added (denoted Q+V). All maps are provided with a full-noise covariance matrix (Jarosik et al. 2007), appropriately corrected for the P06 sky cut and removal of foreground templates. The units used in this paper are thermodynamic μK.

For foreground marginalization, we adopt two individual templates. First, we use the K − Ka difference map, smoothed to 10° FWHM resolution to reduce noise contributions, as a tracer of synchrotron emission. Second, for dust emission we adopt the low-noise template developed by the *WMAP* team for their foreground correction procedure (Page et al. 2007).

We compare our results to the official *WMAP* likelihood code,[11] also available from LAMBDA. To map out the appropriate posteriors, we have written a special-purpose MCMC wrapper around this likelihood code.

4. RESULTS

4.1. *Numerical Verification of the WMAP Likelihood*

The first case considered is that adopted by the *WMAP* likelihood code, namely the co-added QV map. For this analysis, we fix the *EB* and *BB* spectra to zero, and map out the corresponding marginalized *EE* posteriors *l* by *l*, both with the Gibbs sampler and by the *WMAP*-based MCMC code.

The results from this exercise are shown in Figure 1. The agreement between the two approaches is very good, and this is an important validation of the *WMAP* data-processing method: First, we analyze the data at their native $N_{\rm side} = 16$ resolution, while the *WMAP* team analyze maps downgraded to $N_{\rm side} = 8$. Second, they marginalize over a single total foreground template, while we marginalize over the K − Ka difference map and a dust template. Third, we use a Gibbs sampler for the numerical work, while the *WMAP* team uses a brute-force likelihood evaluator. None of these differences affects the low-*l* *EE* spectrum peak visibly, as will be quantified more precisely in the next section.

4.2. *Generalized Analysis*

We now expand the analysis and allow for nonzero *EB* and/or *BB* spectra. We also compute the posteriors for each frequency band separately and jointly. For presentational reasons, we report only band powers in *EE* and *BB* between $l = 2$–6 and $l = 2$–20, respectively. Cases of special interest are treated separately in subsequent sections.

In order to achieve good convergence, 10^6 samples were generated for the nonzero *EB*, $l = 2$–20 cases. For all other cases, 10^5 samples were generated. The CPU time to generate one sample was ~2 s.

The results from these computations are summarized in Table 1. The *EE* posteriors with fixed $EB = BB = 0$ are shown in Figure 2. Again, note the excellent agreement between the *WMAP* results and the QV and Q+V cases in the two top sections.

However, even though the joint QV analyses agree well, the picture is considerably less clear when it comes to single bands and relaxed *EB* constraints. Most importantly, there appears to be more *EE* power in the V-band data than in the Q-band data.

[9] See http://lambda.gsfc.nasa.gov.
[10] See http://healpix.jpl.nasa.gov.
[11] Version v2p2p2.

TABLE 1

MARGINALIZED *EE* AND *BB* BAND POWERS

DATA SET	*EE* POWER (10^{-1} μK^2)		*BB* POWER (10^{-1} μK^2)	
	l = 2–6	l = 2–20	l = 2–6	l = 2–20
EE Free; *EB* = *BB* = 0				
WMAP	$1.1^{+0.9}_{-0.5}$	$0.64^{+0.46}_{-0.34}$	...	...
QV band	$1.2^{+0.9}_{-0.6}$	$0.67^{+0.39}_{-0.38}$	...	...
Q+V band	$1.1^{+0.8}_{-0.6}$	$0.65^{+0.38}_{-0.35}$	...	...
Q band	$1.0^{+1.0}_{-0.8}$	$0.36^{+0.67}_{-0.36}$	...	...
V band	$1.3^{+1.2}_{-0.9}$	$1.2^{+0.9}_{-0.7}$	...	...
EE, *BB* Free; *EB* = 0				
WMAP	$0.94^{+0.76}_{-0.58}$	$0.63^{+0.44}_{-0.37}$	< 0.70	< 0.40
QV band	$1.1^{+0.8}_{-0.6}$	$0.61^{+0.38}_{-0.37}$	< 0.57	< 0.26
Q+V band	$1.1^{+0.8}_{-0.6}$	$0.57^{+0.40}_{-0.31}$	< 0.58	< 0.30
Q band	$0.3^{+1.3}_{-0.3}$	$0.23^{+0.68}_{-0.23}$	$0.3^{+1.2}_{-0.3}$	< 0.71
V band	$1.4^{+1.4}_{-0.9}$	$1.1^{+1.0}_{-0.7}$	< 0.94	< 0.51
EE, *EB*, *BB* Free				
QV band	$1.4^{+0.9}_{-0.7}$	$0.65^{+0.41}_{-0.30}$	$0.30^{+0.60}_{-0.30}$	$0.1^{+0.3}_{-0.1}$
Q+V band	$1.3^{+0.9}_{-0.7}$	$0.66^{+0.43}_{-0.30}$	$0.31^{+0.59}_{-0.31}$	$0.1^{+0.3}_{-0.1}$
Q band	$1.1^{+1.1}_{-0.8}$	$0.54^{+0.65}_{-0.36}$	$0.7^{+1.3}_{-0.6}$	$0.5^{+0.7}_{-0.4}$
V band	$1.8^{+1.6}_{-1.1}$	$1.5^{+0.9}_{-0.9}$	$0.47^{+0.93}_{-0.47}$	$0.4^{+0.6}_{-0.4}$

NOTES.—Values indicate either the posterior mode and upper and lower 68% confidence interval, or the upper 68% confidence limits. If the lower error bar equals the posterior mode value, a nonzero peak is detected, but at a significance of less than 68%.

The *BB* posteriors develop a peak away from $C_l^{BB} = 0$ in the $EB \neq 0$ case. This is not surprising. Since the signal covariance matrix is positive definite, one must have $C_l^{EE} C_l^{BB} > (C_l^{EB})^2$. Therefore, when marginalizing over C_l^{EB}, a nonzero peak emerges in both the *EE* and *BB* spectra individually.

4.2.1. *Foreground Amplitude Posteriors*

In Figure 3 we show the foreground template amplitude posteriors for the Q-, V-, and QV-band data, for the case with fixed $EB = BB = 0$. Although no signs of significant residual foregrounds are observed in the co-added QV band, apparently confirming the fits made by the *WMAP* team, the same is not true for each band individually. On the contrary, nonzero correlations are seen in both the Q- and V-band data individually.

For the Q-band data, the marginal best-fit K − Ka amplitude is $A_s = -0.027^{+0.014}_{-0.17}$, different from zero at 2 σ. The best-fit dust amplitude is $A_d = 15.7^{+8.7}_{-10.7}$. For the V-band data, the best-fit dust amplitude is $A_d = -24.1^{+10.3}_{-11.3}$, 2.3 σ away from zero. The K − Ka amplitude is $A_s = 0.011^{+0.015}_{-0.018}$.

These results may be compared to Table 4 of Page et al. (2007). The main difference between the two analyses is that while we apply the conservative P06 mask to the data, Page et al. (2007) apply the much more aggressive processing mask described by Jarosik et al. (2007). The two analyses remove 26.4% and 5.7% of the sky, respectively. Considering that all cosmological analyses are carried out with the P06 mask, and that variations in the synchrotron spectral index are observed between the Galactic plane and high latitudes (Kogut et al. 2007), it is not immediately clear to us why the more aggressive mask was chosen for this task by the *WMAP* team. The improvement in raw χ^2 after further correcting the "cleaned" *WMAP* maps for these residuals is −5.4 for the Q band and −3.3 for the V band.

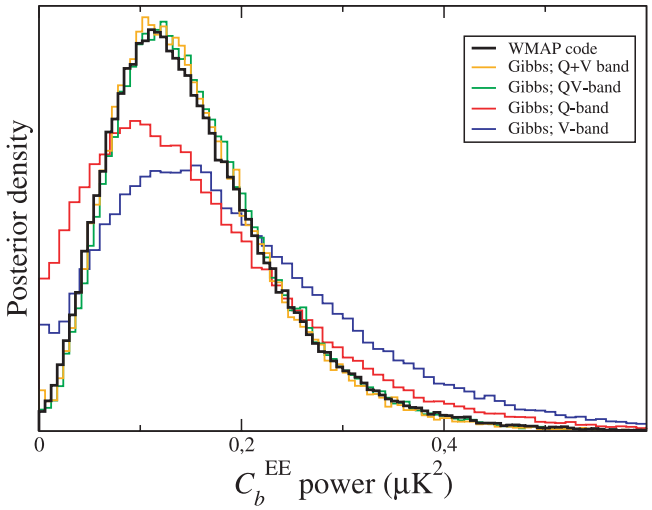

FIG. 2.—Marginal posterior distributions for the *EE* bin power between $l = 2$ and 6.

4.2.2. *E* × *B Cross-Correlation Spectra*

We find evidence for a nonzero *EB* correlation in the V-band sky map. This spectrum is shown in Figure 4 for the Q- and V-band sky maps individually, together with the pseudo-C_l *EB* QV-band spectrum computed by the *WMAP* team. Note the consistently negative correlation observed in the V band. Although the significance of the negative correlation is not more than a few tenths per multipole, and the joint significance is not more than 1–2 σ depending on binning scheme, it is observed consistently in every multipole up to $l = 17$. A similar,

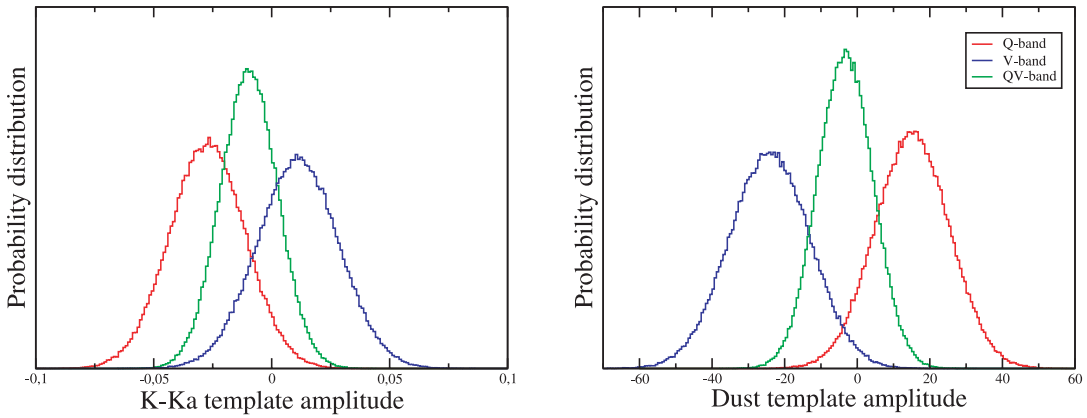

FIG. 3.—Foreground template amplitude marginal posteriors for the Q, V, and QV bands. For this plot, the *EB* and *BB* power spectra were set to zero.

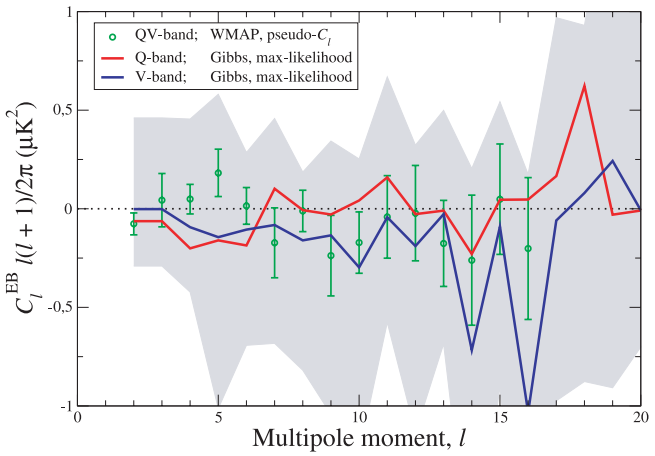

FIG. 4.—$E \times B$ cross-power spectrum. The gray region shows the 1 σ confidence region around the V-band spectrum (*blue curve*); note that the marginal *EB* posterior is strongly non-Gaussian with high kurtosis and heavy tails. The green data points show the *WMAP EB* spectrum computed with a pseudo-C_l estimator with Gaussian error bars; the *WMAP* team explicitly states that these errors are only included as an estimate of the magnitude. The exact treatment yields considerably larger errors, as seen in this plot.

although weaker, trend is seen in the pseudospectrum computed by the *WMAP* team from the QV combination.

5. CONCLUSIONS

We have performed a Bayesian analysis of the low-resolution foreground-corrected 3 yr *WMAP* polarization data using a previously described methodology based on the Gibbs sampler. By doing so, we validated the numerical implementation of the official *WMAP* likelihood code, as well as the *WMAP* team's procedure for degradation of map resolution. However, when generalizing the analysis to allow for nonzero *EB* and *BB* power spectrum components, and also considering individual frequency bands, we found several issues that may be important for the cosmological interpretation of these data.

First and foremost, when relaxing the constraints on *EB* and *BB*, noticeable differences between the Q- and V-band posteriors are observed. Specifically, we find generally more *EE* power in the V-band data than in the Q-band data, but also perhaps some hints of *BB* power in the Q-band data. At the same time, we have also found a negative *EB* correlation in the V-band map, as well as residual foregrounds in both maps.

If these tentative findings are confirmed by future experiments or additional years of *WMAP* observations, significant shifts in cosmological parameters could be the result. For example, if the V-band data alone were used for the *WMAP* 3 analysis instead of the QV combination, the amplitude of the $l = 2$–6 *EE* detection would increase by 20%–50%, depending on whether *BB* is allowed to vary or not. Consequently, τ could increase from 0.09 to ~0.12, and n_s by a percent or two, comparable to its current nominal statistical uncertainty of 0.015, from ~0.97 to ~0.98.

As discussed in the introduction, systematics are a serious concern for both the temperature and polarization data for both τ and n_s. It is important to bear in mind that the currently quoted uncertainties on these quantities often found in the literature are statistical only. The unknown systematic uncertainties may turn out to be nonnegligible for the currently available data sets, and, in particular, we believe it is too early to draw any firm conclusions concerning the precise value of n_s. Fortunately, *Planck* will clarify these issues in the near future.

We wish to thank David Larson for his contributions during the early phases of this project. We acknowledge use of the Legacy Archive for Microwave Background Data Analysis (LAMBDA). We acknowledge use of the HEALPix software (Górski et al. 2005) and analysis package for deriving the results in this paper. This work was partially performed at the Jet Propulsion Laboratory, California Institute of Technology, under a contract with the National Aeronautics and Space Administration. H. K. E. acknowledges financial support from the Research Council of Norway. B. D. W. acknowledges support by NSF grant 0507676, the Friedrich Wilhelm Bessel Research Prize by the Alexander v. Humboldt foundation, and NASA subcontract 1236748.

REFERENCES

Eriksen, H. K., et al. 2004, ApJS, 155, 227
———. 2006, ApJ, 641, 665
Gelfand, A. E., & Smith, A. F. M. 1990, J. Am. Statis. Assoc., 85, 398
Górski, K. M., Hivon, E., Banday, A. J., Wandelt, B. D., Hansen, F. K., Reinecke, M., & Bartelmann, M. 2005, ApJ, 622, 759
Hinshaw, G., et al. 2007, ApJS, 170, 288
Huffenberger, K. M., Eriksen, H. K., & Hansen, F. K. 2006, ApJ, 651, L81
Jarosik, N., et al. 2007, ApJS, 170, 263
Jewell, J., Levin, S., & Anderson, C. H. 2004, ApJ, 609, 1
Kogut, A., et al. 2007, ApJ, 665, 355
Larson, D. L., Eriksen, H. K., Wandelt, B. D., Górski, K. M., Huey, G., Jewell, J. B., & O'Dwyer, I. J. 2007, ApJ, 656, 653
Page, L., et al. 2007, ApJS, 170, 335
Spergel, D. N., et al. 2007, ApJS, 170, 377
Wandelt, B. D., Larson, D. L., & Lakshminarayanan, A. 2004, Phys. Rev. D, 70, 083511